Self-consistent parametrization of DFT + U framework using linear response approach: Application to evaluation of redox potentials of battery cathodes

Maxim Shishkin[1,*] and Hirofumi Sato[1,2]

[1]*Elements Strategy Initiative for Catalysts and Batteries (ESICB), Kyoto University, Katsura, Kyoto 615-8520, Japan*

[2]*Department of Molecular Engineering, Kyoto University, Nishikyo-ku, Kyoto 615-8510, Japan*

(Received 18 November 2015; revised manuscript received 24 January 2016; published 24 February 2016)

The accuracy of DFT + U calculations, applied to the study of electronic structure and energetics of strongly correlated materials, heavily depends on U parameters, chosen for adequate treatment of d and f states. Computational evaluation of U parameters, which does not require fitting to experimental measurements or results of computationally expensive schemes, is highly desirable for the study of novel materials and even more so for materials not yet synthesized to date. Within this work, we show that the linear response method could provide U parameters which can yield redox potentials of battery cathode materials in much better agreement with experiment than conventional density functional theory (DFT). In our approach, we evaluate U values self-consistently, ensuring agreement between U calculated using linear response with the value used for DFT + U calculations. We find that such self-consistency is necessary for determination of adequate values of U. We also studied the impact of using various PAW (projector augmented wave) potentials for transition-metal ions, that differ by the number of electrons treated as valence. We find that redox potentials are reasonably well reproduced for all cases, although a slightly higher degree of accuracy corresponds to PAW potentials with semicore electrons treated as valence. Importantly, we find that converged values of U are substantially different for various PAW potentials of transition-metal ions of the same material. Overall, we find that self-consistent DFT + U/linear response calculations provide quite accurate values of redox potentials for materials with purely ionic bonding (e.g., $LiFePO_4$, $LiCoPO_4$, $LiCoO_2$, $LiMnPO_4$, $NaFePO_4$), whereas for materials with covalent pd hybridization (e.g., $LiNiO_2$) or conducting materials (e.g., $LiTiS_2$) the agreement with experimental redox voltage is lower. This emphasizes the need for application of more advanced techniques (e.g., DFT + U + V method) for accurate study of partially covalent and metallic materials, which contain transition-metal ions.

DOI: 10.1103/PhysRevB.93.085135

I. INTRODUCTION

In its original formulation, density functional theory (DFT) emerged as a scheme designed for calculations of exact total energies of atomic systems, provided that exact exchange-correlation potential is known [1–3]. Although no formal justification exists for interpreting single-electron DFT energies as observables [4], the density of states of solids [5,6] and even excited states of finite systems [7] can be calculated in a reasonable agreement with experiment when DFT or its extensions (e.g., time-dependent DFT, ΔSCF) are employed. On the other hand, in spite of a reputation of a ground-state theory, DFT calculations, based on now traditional local density (LDA) [8] and generalized gradient (GGA) [9] approximations, do not always provide accurate values of total energies. As an example, LDA/GGA formation energies of silicon self-interstitials are underestimated by more than 1 eV when compared to the results of more accurate quantum Monte Carlo technique or experiment [10]. Moreover, the accuracy of calculations that involve total energy differences (e.g., enthalpy of materials formation, surface free energies, diffusion barriers, etc.) is particularly poor for strongly correlated materials, with elements that contain d and f electrons [11]. For instance, it has been demonstrated recently that although formation enthalpies of metallic alloys can be computed in good agreement with experiment [12], for the case of semiconductors and insulating materials LDA/GGA yield rather overestimated values of enthalpies of formation [13].

Two types of methods are usually used to allow for at least partial correction of LDA and GGA deficiencies in practical calculations of modern materials science. These are the hybrid functionals approach [14] and Hubbard corrected DFT + U method [15]. Unlike very accurate quantum chemistry or quantum Monte Carlo techniques, these two methods offer a reasonable compromise between computational cost and precision. It should be noted that due to inclusion of nonlocal Hartree-Fock exchange, hybrid functional calculations are inherently slower computationally than conventional local DFT. Moreover, the accuracy of HSE06 hybrid functional calculations [14], which are usually applied in condensed matter studies, is not necessarily higher than those of more computationally robust DFT + U [16]. On the other hand, DFT + U is featured by a proven record of substantial improvement over conventional DFT in prediction of energetics and electronic structure of strongly correlated materials. Additionally, as a Hubbard correction term of DFT + U method is determined by the elements of occupation matrix (see discussion in Sec. II A), such DFT + U calculations are characterized by only a marginal increase in computational cost, as compared to conventional LDA and GGA calculations.

From a computational viewpoint, the challenge associated with application of a DFT + U approach is the need for determination of a U parameter. Indeed, similar to DFT, where exchange-correlation potential has to be approximated (e.g., LDA/GGA), the DFT + U correction term contains a numerical U parameter, which value is usually derived by fitting the computational results either to experimental measurements [17] or the findings of other calculations (e.g.,

*Corresponding author: shishkin.maxim.6c@kyoto-u.ac.jp

hybrid functionals [18]). Such fitting to experimental findings is problematic for materials, where available experimental data are insufficient, which is often the case for novel materials and even more so for materials that are not yet synthesized to date. An alternative approach of fitting of DFT + U results to the findings of other (usually more computationally costly) calculations can also be problematic if the size of a minimal computational cell of a material is large (e.g., >100 atoms). In any case, fitting to a certain property of interest (e.g., forbidden gap) does not necessarily result in better prediction of other properties (formation or binding energies). Therefore, evaluation of U parameters from first principles is highly desirable.

In an attempt to classify currently proposed methods, used for first-principles evaluation of U parameters, we divide them into three groups. The first group of methods exploits expression of U either through double derivatives of total energy over single-electron density and magnetization [19] or first derivatives of a single-electron energy over localized electron density [20–22]. The linear response scheme that is used for producing variation of electron density for subsequent calculation of density derivative is further discussed in Sec. II B. Within the second group of methods, the expressions of U and J parameters are derived analytically, postulating that onsite Hubbard term of DFT + U is equal to a sum of Coulomb and exchange contributions of Hartree-Fock energy [23]. The computationally enhanced schemes that stem from this original idea have been proposed subsequently [24,25]. The constrained random phase approximation (cRPA) approach, which constitutes the third group of methods, relies on a notion that the U parameter can be viewed as screened electron-electron Coulomb interaction, where screening is introduced by multiplying Coulomb potential by the inverse dielectric matrix [26–28]. Similar to many body GW approximation, which includes screened exchange potential, the U parameter is mapped as an integral over Coulomb potential, dielectrically screened by nonlocalized (e.g., excluding d electrons) states. As the dielectric matrix used for screening is a function of frequency ω, the value of U is calculated for static case when $\omega = 0$ [26].

Comparison between the conceptual differences and performance of these three approaches has been made in the past [26,29]. Generally, these techniques do not provide similar values of U parameters for a chosen material and no consensus exists for favoring one method over the other. Such controversy is not so surprising as the last two groups of methods are essentially based on adjusting the U parameter so that the Hubbard term can closely reproduce either HF or RPA electron-electron contributions. It should be noted that both HF and RPA methods are not exact, as higher terms of respective many-body theories are required for exact solution. Thus, different values of U obtained from respective techniques are actually caused by different treatment of electron-electron interactions in HF and RPA methods. From a computational perspective, application of the second group of methods is encumbered by somewhat complex evaluation of Coulomb and exchange integrals for periodic systems [24,25], whereas the third group of methods is plagued by the need of calculation of time-consuming quantities such as polarizabilities and dielectric matrices in the RPA technique [26]. In contrast, the first group of methods, particularly those employing linear response, are quite computationally robust with associated computational cost similar to DFT or DFT + U calculations.

The linear response approach has been initially applied for evaluation of ground-state properties of transition-metal oxides (e.g., phase transitions of NiO [22]) as well as calculations of redox potentials of various transition-metal compounds, which find application as cathode materials in Li-ion batteries [21]. In these seminal papers, U parameters have been evaluated using linear response functions of conventional DFT(GGA)density. For redox potential calculations in Ref. [21], the linear response evaluation of U has been carried out using implementation in QUANTUM ESPRESSO code [30], whereas DFT + U calculations have been subsequently performed using the VASP program [31]. It should be noted that this is the practice often followed in the works where U parameters have been derived using the linear response approach. More recently, further extensions of linear response methods have been proposed [32]. These include self-consistent evaluation of U parameters within DFT + U framework [33], inclusion of magnetic (exchange) interaction with the help of effective J parameter (DFT + U + J method) [34], and addition of interactions of localized (e.g., d) electrons with sp states of the same and adjacent ions of the cell (DFT + U + V method) [35].

In this work, we performed self-consistent evaluation of U parameters, ensuring that the value, determined by linear response, agrees with the one used in DFT + U calculations. As already mentioned, this extension of the method has been proposed earlier [33], but application has been mostly confined to molecules. In our work we apply self-consistent evaluation of U for DFT + U study of solids. Additionally, unlike a common approach where U is evaluated using implementation of linear response scheme in QUANTUM ESPRESSO, we present a more rigorous scheme where U parameters are evaluated using VASP code for their subsequent application in DFT + U calculations using the same VASP package. Apart from convenience of using the same program for coupled linear response/DFT + U calculations, we believe that this approach is more accurate due to potential incompatibility of U if linear response and DFT + U calculations are performed using different codes. Indeed, differences in employed pseudopotentials or projector augmented wave (PAW) potentials, such as different potential radii or number of electrons treated as valence, can cause inadequacy of U obtained using the linear response method for subsequent application in DFT + U calculations.

The outline of this work is as follows. In Sec. II, we provide a brief overview of the DFT + U scheme and present the details of the linear response method. In Sec. III, we provide discussion of redox processes in Li- and Na-battery cathodes and give definition of a cathode redox potential. In Sec. IV, we present the results of calculations of redox potentials performed using coupled linear response/DFT + U method. We discuss electronic structure of studied materials and analyze the accuracy of calculated redox potentials. In Sec. V, we provide a discussion of computational aspects of the employed linear response scheme. In particular, we discuss convergence of U parameters (self-consistency), linearity of density variation with respect to applied potential, and the impact of chosen PAW potentials on redox potentials and the self-consistently converged values of U. In Sec. VI, we

perform comparison of our results (i.e., redox potentials) with previously published data. Conclusions are provided in Sec. VII.

II. METHODOLOGY DESCRIPTION

A. DFT + U method

The DFT + U energy can be evaluated as a local DFT energy augmented by Hubbard contribution minus double-counting correction term [32]

$$E^{\mathrm{DFT}+U}[n(\mathbf{r})] = E^{\mathrm{DFT}}[n(\mathbf{r})] + E^{\mathrm{Hub}}[n^{I\sigma}] - E^{\mathrm{DC}}[N^{I\sigma}]. \quad (1)$$

The Hubbard contribution is added to account for exchange-correlation effects, associated with localized d or f orbitals, whereas the double-counting term is subtracted for removal of exchange-correlation effects, already introduced on the LDA or GGA level. In this work, we adopt the widely used rotationally invariant formulation of DFT + U framework [36], within which the combined contribution of Hubbard and double-counting correction terms has a concise form

$$E^{U}[n^{I\sigma}] = \sum_{I,\sigma} \frac{U^I}{2} \mathrm{Tr}[n^{I\sigma}(1 - n^{I\sigma})]. \quad (2)$$

In Eq. (2), the elements of occupation matrices, constructed via projection of valence bands on localized (e.g., d) orbitals on respective ions, are expressed as

$$n^{I\sigma}_{mm'} = \sum_{\mathbf{k},v} f^{\sigma}_{\mathbf{k},v} \left\langle \psi^{\sigma}_{\mathbf{k},v} \right| P^{I}_{mm'} \left| \psi^{\sigma}_{\mathbf{k},v} \right\rangle, \quad (3)$$

where I, σ, and m are the number of an ion, the spin number, and magnetic number, respectively. $|\psi^{\sigma}_{\mathbf{k},v}\rangle$ are valence bands, determined by periodic plane wave calculations, $P^{I}_{mm'}$ is a projector operator on localized (e.g., d) orbitals, and $f^{\sigma}_{\mathbf{k},v}$ are occupation weights of valence states $|\psi^{\sigma}_{\mathbf{k},v}\rangle$. The projector operator is defined as

$$P^{I}_{mm'} = \left|\phi^{I}_{m}\right\rangle \left\langle \phi^{I}_{m'}\right|, \quad (4)$$

where $|\phi^{I}_{m}\rangle$ are d orbitals, localized on atom I. Using the expression for the energy of a Hubbard term [Eq. (2)], the Hubbard contribution to local Hamiltonian can be obtained as

$$V_{\mathrm{Hub}} \left|\psi^{\sigma}_{\mathbf{k},v}\right\rangle = \sum_{I,m,m'} U^I \left(\frac{1}{2}\delta_{mm'} - n^{I\sigma}_{mm'}\right) \left|\phi^{I}_{m'}\right\rangle \left\langle \phi^{I}_{m} \middle| \psi^{\sigma}_{\mathbf{k},v}\right\rangle. \quad (5)$$

In a rotationally invariant scheme, employed herein [36], a single U parameter is required for application of such formalism in contrast to originally proposed DFT + U schemes where two parameters (U and J) are employed [19]. Such approximation is often justifiable and therefore a fully rotationally invariant scheme [37] and a somewhat simplified rotationally invariant method usually yield very similar results. However, for materials with pronounced noncollinear magnetism, a fully rotationally invariant scheme might be preferential as it potentially allows more accurate description of magnetic properties due to appropriate tuning of J parameter [34].

In this work, we have employed the PAW approach [38] which has been extended to DFT + U framework using implementation by Bengone and co-workers into VASP code [39]. For computational purposes, two types of electronic wave functions are introduced in PAW framework. These are pseudo (PS) and all-electron (AE) wave functions (or bands), denoted as $|\tilde{\Psi}\rangle$ and $|\Psi\rangle$, respectively. The PS bands are computationally convenient as they are expanded in plane waves. However, the square of the modulus of PS bands (density) does not have a physically meaningful character in the vicinity of the nucleus (core region). Therefore, in construction of AE bands (with the respective square of the modulus corresponding to meaningful electronic density both in the core and interatomic regions), the PS functions have to be augmented by the projector containing term

$$|\Psi\rangle = |\tilde{\Psi}\rangle + \sum_{\Lambda} [|\phi_{\Lambda}\rangle - |\tilde{\phi}_{\Lambda}\rangle] \langle \tilde{p}_{\Lambda} | \tilde{\Psi}\rangle, \quad (6)$$

where $|\phi_{\Lambda}\rangle$ and $|\tilde{\phi}_{\Lambda}\rangle$ are all-electron and pseudo partial waves, whereas $|\tilde{p}_{\Lambda}\rangle$ are projector functions. $|\tilde{\phi}_{\Lambda}\rangle$ are used for expanding PS bands in the core region on a course regular grid, whereas $|\phi_{\Lambda}\rangle$ are used for expanding the AE band in the core region on a fine radial support grid. The projector functions $\langle \tilde{p}_{\Lambda}|$ are used for determining the projection coefficients of PS bands on the set of pseudopartial waves $|\tilde{\phi}_{\Lambda}\rangle$ (they are defined on the same regular grid). The transformation (6) is crucial in the PAW method, as it allows reconstruction of the PS band into the AE band in the core region Λ, whereas in the interatomic region the PS and AE bands coincide. Further details about the PAW method can be found in original works [38,40,41] as well as review papers that have been published on this subject [42–44].

Bengone *et al.* have shown that occupation matrix within PAW formalism can be evaluated as

$$n^{I\sigma}_{mm'} = \sum_{\mathbf{k},v} f^{\sigma}_{\mathbf{k},v} \left\langle \tilde{\Psi}^{\sigma}_{\mathbf{k},v} \right| \tilde{P}^{I}_{mm'} \left| \tilde{\Psi}^{\sigma}_{\mathbf{k},v} \right\rangle. \quad (7)$$

Formally very similar to Eq. (3), the occupation matrix expression includes a so-called pseudoversion projector operator $\tilde{P}^{I}_{mm'}$ (we employ terminology introduced in the work of Bengone *et al.*). The pseudoversion projector operator $\tilde{P}^{I}_{mm'}$ is related to a more common projector $P^{I}_{mm'}$ [Eq. (4)] as

$$\tilde{P}^{I}_{mm'} = \sum_{\Lambda,\Lambda'} |\tilde{p}_{\Lambda}\rangle \langle \phi_{\Lambda}| P^{I}_{mm'} |\phi_{\Lambda'}\rangle \langle \tilde{p}_{\Lambda'}|. \quad (8)$$

Using Eq. (7) for occupation matrix and Eq. (8) for projector operator, the Hubbard correction term within PAW formalism can be defined as

$$V_{\mathrm{Hub}} \left|\tilde{\psi}^{\sigma}_{\mathbf{k},v}\right\rangle = \sum_{I,m,m'} U^I \left(\frac{1}{2}\delta_{mm'} - n^{I\sigma}_{mm'}\right) \times \sum_{\Lambda,\Lambda'} |\tilde{p}_{\Lambda}\rangle \langle \phi_{\Lambda}| P^{I}_{m'm} |\phi_{\Lambda'}\rangle \left\langle \tilde{p}_{\Lambda'} \middle| \tilde{\psi}^{\sigma}_{\mathbf{k},v}\right\rangle. \quad (9)$$

In the above expression, the occupation matrix elements are evaluated using Eqs. (7) and (8), rather than (3). It is clear that the Hubbard energy, equal to the expectation value of operator (9), is identical to the one defined in Eq. (2).

B. Linear response method

Evaluation of the U parameter can be performed relying on definition of U as a difference of double derivatives of

total energy over density for the interacting and noninteracting multielectronic system:

$$U = \frac{\partial^2 E^{\text{int}}}{\partial q_I^2} - \frac{\partial^2 E^{\text{non}}}{\partial q_I^2}, \tag{10}$$

where q_I is a variation of an electron density, localized on atom I [22]. The second energy derivative with respect to density which corresponds to noninteracting (or bare) case is subtracted in order to evaluate effective electron-electron interaction kernel using the linear response approach [45,46]. Equivalently, U can be expressed as the difference of the first derivatives of localized electron energies with respect to density for noninteracting and interacting systems:

$$U = \frac{\partial {\alpha_I}^{\text{non}}}{\partial q_I} - \frac{\partial {\alpha_I}^{\text{int}}}{\partial q_I}. \tag{11}$$

In this work, we performed evaluation of U using the second approach, i.e., via calculation of the first derivative of a single-electron energy with respect to density. The task is translated into determination of a variation of a single-electron energy in response to the change of the electronic density. Such perturbation can be studied using the constrained DFT method, where desired charge density distribution can be imposed for subsequent evaluation of the change of electronic energies [47]. However, a backward approach, where single-electron energy can be shifted, causing variation of a charge distribution, can also be applied. A linear response approach provides such alternative route. The U parameter is evaluated as the difference of diagonal elements of the inverse response functions for noninteracting and interacting systems:

$$U = \left(\chi_{\text{non}}^{-1} - \chi_{\text{int}}^{-1}\right)_{II} \tag{12}$$

with response function generally defined as

$$\chi_{IJ} = \frac{\partial n_I}{\partial \alpha_J}. \tag{13}$$

The response function is a matrix where indices I and J correspond to an atom on which perturbation is applied (J) and an atom, where variation of density is evaluated (I) whereas α is a variation of energy levels of localized electrons. The derivative in Eq. (13) is evaluated using linear response approach. To obtain a variation of atomic density, the projector operator, defined in Eq. (4), is multiplied by a coefficient α and added/subtracted to/from DFT or DFT + U Hamiltonian:

$$H_{\text{pert}} = H_0 \pm \alpha \sum_m \left|\phi_m^I\right\rangle\left\langle\phi_m^I\right|. \tag{14}$$

In Eq. (14), we introduce perturbed (H_{pert}) and standard DFT/DFT + U (H_0) Hamiltonians. The projector operator in Eq. (14) is applied to the states, localized on atom I. Summation over all magnetic (m) numbers is performed. Positive and negative signs for the projection operator in Eq. (14) (α is a positive number) correspond to up shift or down shift of energy levels of states, localized on atom I. Upon solution of the system of Eq. (14), the new occupation matrices can be calculated using Eq. (3).

Calculation of response function, using Eq. (13), is straightforward: the difference between perturbed and initial occupancy of localized electrons has to be divided by coefficient α. As this is a derivative calculation, in theory an infinitesimal value of α should be used. In practical calculations, small values in the range of 0.1–0.2 eV are usually employed (this aspect is further discussed in Sec. V).

As has been mentioned, the response functions [Eq. (13)] have to be calculated for the interacting and noninteracting cases. The interactive response is obtained via solution of Eq. (14) with update of the density, used for construction of the local potentials of DFT/DFT + U Hamiltonians [Coulomb and exchange-correlation terms as well as Hubbard correction (5) for the DFT + U calculations]. The noninteractive response can be obtained by fixing the density used for construction of Hamiltonian in Eq. (14). This corresponds to the first iteration in solution of Eq. (14) within self-consistent cycle, prior to the first density update.

Before ending this section, we need to present an expression for the perturbed Hamiltonian [Eq. (14)], formulated within PAW framework. Using definition of projector in Eq. (8), we land into the following expression:

$$H_{\text{pert}} = H_0 \pm \alpha \sum_m \sum_{\Lambda,\Lambda'} \left|\tilde{p}_\Lambda\right\rangle \left\langle\phi_\Lambda\right| P_{mm}^I \left|\phi_{\Lambda'}\right\rangle \left\langle\tilde{p}_{\Lambda'}\right|. \tag{15}$$

The determination of U within the PAW formalism is performed exactly the same way as has been outlined above for standard case [with the occupations of localized states evaluated using Eq. (7)].

III. COMPUTATIONAL DETAILS

A. Redox potential evaluation

Reduction and oxidation (redox) processes are at heart of operation of electrochemical devices such as batteries or fuel cells. Redox cycling occurs as a result of addition and removal of negative charge (electrons) in/from insulating materials (e.g., oxides), caused by change of the material stoichiometry. In Li- and Na-ion batteries, adding or removal of Li^+ or Na^+ cations into/from electrode bulk (so-called intercalation and deintercalation processes) results in addition or removal of respective number of electrons to/from the electrode. Evaluation of a redox potential at a given concentration of charge carrier ions (Li or Na) would require averaging over possible positions of these ions, making numerical determination of voltage profiles too computationally demanding. In this work, we performed evaluation of the so-called average redox potentials, where the need of averaging over positions of charge carrier ions can be eliminated as is discussed in the following.

The average redox potential of a cathode material (e.g., transition metal oxide) is defined as

$$\Phi_r = -\frac{1}{e}\int_{x_1}^{x_2} \frac{\mu_{\text{Li}}^{\text{cath}}(x) - \mu_{\text{Li}}^0}{x_2 - x_1} dx, \tag{16}$$

where $\mu_{\text{Li}}^{\text{cath}}$ and μ_{Li}^0 are chemical potentials of Li ions in the cathode and Li bulk, respectively; x_1 and x_2 set the limits of a change of Li concentration in the cathode during redox process; e is a single-electron charge [48]. For practical calculations of redox potentials, the above expression is normally approximated as

$$\Phi_r \cong -\frac{E^{\text{cath}}(x_2) - E^{\text{cath}}(x_1) - (x_2 - x_1)E^{\text{Li}}}{e(x_2 - x_1)}. \tag{17}$$

In Eq. (17), $E^{\text{cath}}(x_2)$ and $E^{\text{cath}}(x_1)$ are the total energies of cathode material cell, averaged over possible configurations at Li concentration of x_2 and x_1 respectively, whereas E^{Li} is the energy of a Li atom, determined as a total energy of Li formula unit, divided by the number of constituent Li atoms. This is a quite reasonable approximation of Eq. (16), as the free-energy differences of bulk phases can be safely approximated by enthalpy differences due to the negligibly small contributions of pressure and entropy-dependent terms [48].

In this work, we performed evaluation of the average redox potentials, that correspond to the change of Li or Na concentration from 0% to 100%. Following Eq. (17), these can be evaluated as

$$\Phi_r = -\frac{E^{\text{cath}}(N) - E^{\text{cath}}(0) - N E^{\text{Li}}}{eN}, \tag{18}$$

where N is a maximum total number of Li or Na ions present in a computational cell of cathode material. As a single number, rather than a function of Li or Na concentration, such potential offers a useful and concise characterization of a cathode operating voltage. Moreover, no averaging over total energies of possible configurations at each concentration (x_1 and x_2) is required in this case, limiting the number of studied atomic systems to three (e.g., LiMO_2, MO_2, and Li where M is a transition-metal ion). We wish also to note that for brevity in subsequent sections we refer to average redox potentials as simply redox potentials, as within this work we did not perform any study of actual redox potential at specific concentrations of charge carrier ions.

The total energies of the intercalated and deintercalated materials, present in Eq. (18), were evaluated with the help of DFT + U calculations. Respective values of U parameters for intercalated and deintercalated structures, determined by linear response calculations, have been employed.

B. Structure of studied cathode materials

Within this work we performed evaluation of average redox potentials [Eq. (18)] for seven cathode materials with well-characterized structural properties and available experimentally measured redox potentials. Each of the studied materials adopt either olivine or layered type of crystal structure, shown in Fig. 1 (both intercalated and deintercalated structures, that can be interchanged via redox process are presented). Materials with layered structure are transition-metal oxides and one sulfide ($LiNiO_2$, $LiCoO_2$, and $LiTiS_2$), whereas phosphates ($LiFePO_4$, $LiMnPO_4$, $LiCoPO_4$, and $NaFePO_4$) adopt the olivine structure. For all intercalated structures, we used the lattice constants and atomic coordinates, provided by experimental measurements. We carried out optimization of the lattice constants and then using these theoretical values, we performed optimization of atomic positions for all structures. For deintercalated structures, we performed optimization of experimental lattice constants, if these were available. For the cases where we did not succeed in finding the reports on experimentally studied deintercalated structures, we performed optimization of lattice constants by removing the Li/Na ions from intercalated models. Atomic positions were subsequently optimized.

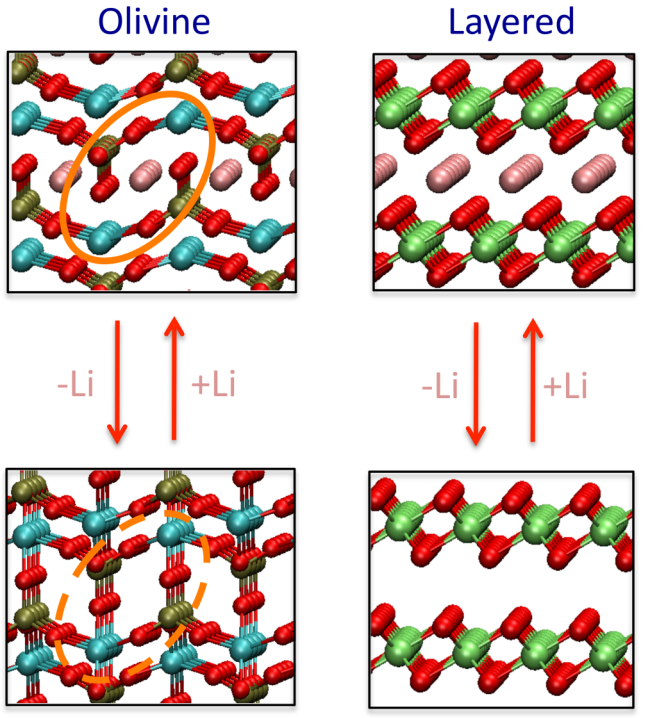

FIG. 1. Two types of studied structures: olivine and layered. Red circles correspond to oxygens, light gray to Li ions. Redox process occurs through removal and addition of Li atoms, shown by vertical arrows. For phosphates (olivine structure), phosphorous is indicated by brown circles whereas transition-metal ions (Fe, Mn, and Co) are shown as light cyan circles. In layered materials, transition metals (Fe, Ni, Co, and Ti) are indicated as green circles.

For all calculations, we have employed the cutoff energy of 600 eV. The convergence with regard to the number of k points has been checked, ensuring well-converged values of redox potentials (below 0.01 V). We used the PBE exchange-correlation functional [49] for DFT calculations and PAW potentials for all types of ions in the supercells. For transition metals (Fe, Ni, Co, Mn, Ti), we used two types of PAW potentials, available from the VASP library: potentials with the lowest possible number of electrons treated as valence (outward electron shell) and potentials with additional semicore electrons also treated as valence. For convenience of reference, we term these PAW potentials as PAW_{min} and PAW_{max}, respectively.

In this work, we used supercells with the following characteristic sizes of intercalated structures: 112 atomic cells for phosphates, 108 atomic cells for oxides, and 72 atomic cell for a sulfide. Although such computational cells should be sufficiently large to yield converged values of redox potentials with respect to the cell size (see discussion on this subject in Ref. [22]), we have verified that further increase of the cell size provides well-converged values of U parameters. Indeed, using $LiFePO_4$ as an example, we found that the U parameter changes within 0.01 eV, when we double respective cell size.

IV. ANALYSIS OF CALCULATED REDOX POTENTIALS

In this section, we present the results of calculations of redox potentials together with the analysis of electronic

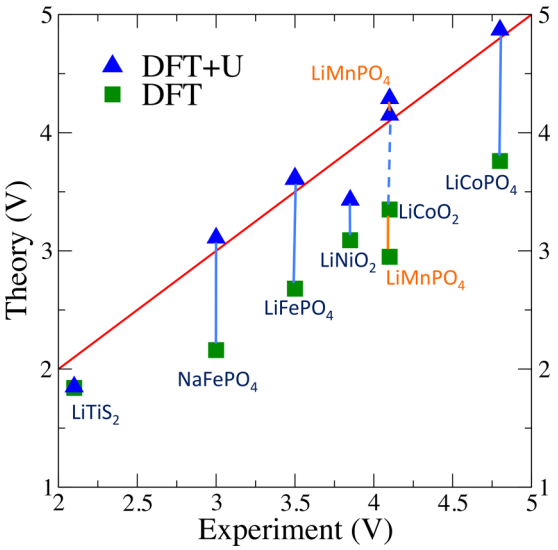

FIG. 2. Redox potentials, calculated using Eq. (18), are presented for comparison of theoretical values (DFT + U and DFT) with experimental measurements. In the ideal case, the theoretically calculated value is positioned on a sloped red line (this corresponds to complete agreement with experiment).

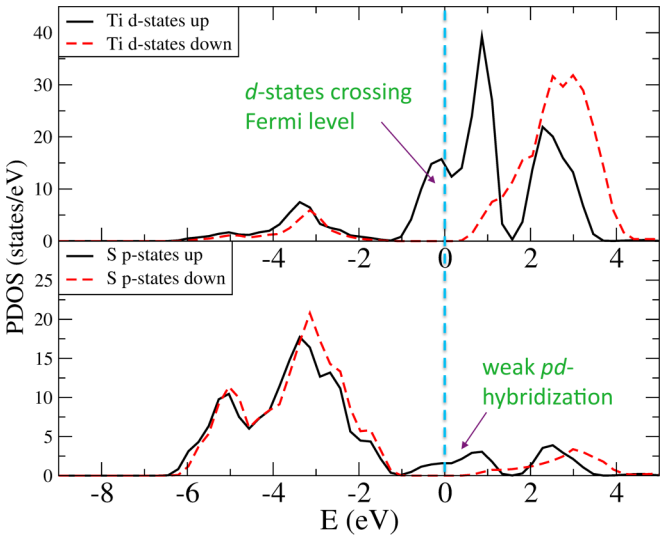

FIG. 3. PDOS of $LiTiS_2$, calculated using DFT + U method. Top: PDOS of d states of Ti; bottom: p states of sulfur. Metallic character is observed due to crossing of Fermi level (broken line) by PDOS of d states of Ti.

structure of studied materials, using PAW_{max} potentials for transition-metal ions. U parameters have been evaluated using self-consistent linear response/DFT + U approach. Additionally, we also rely on a simplified method for determination of U parameter, where U is determined by setting to zero the off-diagonal elements of the self-consistent and non-self-consistent response functions in Eq. (13). In the next section, we address how other types of PAW potential of transition-metal atoms (PAW_{min}) can vary the magnitude of calculated redox voltage. In Sec. V, we also provide a discussion of the impact of neglecting the off-diagonal elements of linear response matrix on the resultant value of U.

The calculated redox potentials, which were obtained using DFT + U and DFT methods, are presented in Fig. 2. Comparison with experimental measurements is also provided. With exception of $LiTiS_2$, DFT (PBE in our case [49]) derived redox potentials are significantly lower than experimental values (by about 1 V). A reasonable agreement of redox potential of $LiTiS_2$ with experimental value can be explained by metallic character of this material. As we have mentioned in the Introduction, for metals, the quantities, which involve total energy differences (e.g., formation energies), are calculated in a good agreement with experiment. This trend is not that surprising as widely used local functionals (LDA and GGA) have been derived to reproduce the ground state of a quasihomogeneous electronic gas, which distribution character is quite similar to the delocalized distributions of itinerant electrons in metals. For the oxides and phosphates, where DFT wrongly predicts delocalized distribution of d states of transition metals and metallic character of density of states (absence of a gap), additional corrections for computational procedure are clearly needed.

Applying DFT + U calculations to these materials, we obtained substantially improved values of theoretical redox potentials, which are higher in energy as compared to DFT-based findings (Fig. 2). Remarkably that for the case of $LiTiS_2$, DFT + U calculations provide a slightly improved redox potential, in spite of itinerant distribution of Ti d states. Moreover, the PDOS of d states of Ti, evaluated using DFT + U method, crosses Fermi level, thus demonstrating that DFT + U calculations still predict metallic character of this material in agreement with experiment (Fig. 3). This finding is important as it shows that when the U parameter is evaluated with the linear response method using self-consistent scheme, the DFT + U calculations do not lead to a pitfall of incorrect prediction of insulating character of a material, which is experimentally known to be a conductor. On the other hand, in case of a conducting material, the fully localized limit (FLL) of DFT + U approach, used herein, might be less suitable than the around mean field (AMF) approximation, specifically designed for description of delocalized electronic states [50]. Application of the AMF approach for the study of weakly correlated materials has been performed in the past [51,52]. Moreover, a computational scheme that allows a linear interpolation between FLL and AMF approaches with respective weight coefficients, evaluated from the first principles [53], might be an interesting alternative for future studies of conducting and possibly covalent materials.

For five out of six oxide and phosphate materials, DFT + U calculations yield very accurate values of redox potentials (with $LiNiO_2$ being an exception here). At first, we shall analyze these five cases. Figure 4 provides a comparison of partial density of states (PDOS) of d electrons of Fe atoms and p electrons of O atoms of $LiFePO_4$ for DFT (Fig. 4, top) and DFT + U (Fig. 4, bottom) calculations. The calculations have been performed for antiferromagnetic configuration of $LiFePO_4$, as earlier reports found that this magnetic ordering leads to the lowest energy for this material [21]. In Fig. 4 (top), we find that DFT calculations predict a metallic character of $LiFePO_4$, as d band of Fe crosses the Fermi level. In contrast, addition of Hubbard correction leads to formation of a gap,

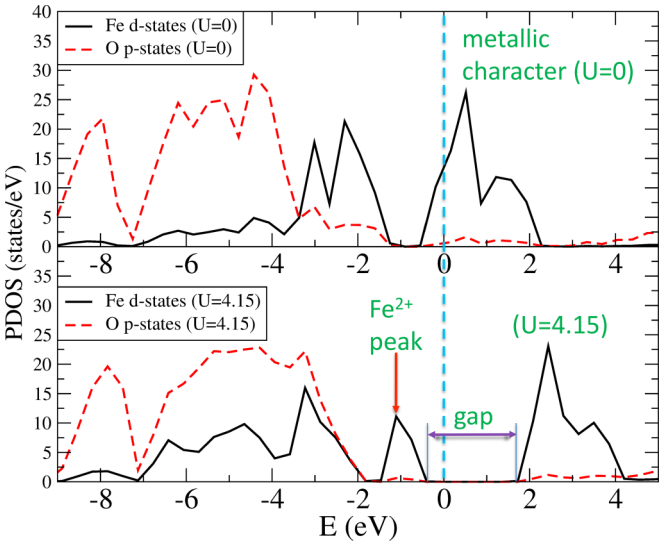

FIG. 4. PDOS of $LiFePO_4$, calculated using DFT method (top) and DFT + U method (bottom). DFT calculations predict metallic character of this material (PDOS of d states of Fe crosses Fermi level, indicated by the broken line). DFT + U method predicts opening of the gap (bottom figure). A characteristic peak (Fe^{2+}), which corresponds to d states of Fe for intercalated state, is highlighted.

shown in Fig. 4 (bottom). Moreover a characteristic peak in PDOS of d electrons of Fe (denoted as Fe^{2+} in Fig. 4, bottom) appears when DFT + U calculations are applied in agreement with the results of experimental measurements [54].

We find that although DFT + U correctly predicts presence of a gap, the width of this gap (~2 eV) is still well below the experimentally measured value of 3.7 eV [54]. Another example is $LiCoO_2$, where the band gap of 2.3 eV is evaluated using our DFT + U calculations, whereas potentially more accurate DFT + U/G_0W_0 calculations predict a wider gap of ~3 eV [55]. Thus, we observe only a qualitative improvement in description of electronic structure of insulating material when Hubbard correction is added to DFT Hamiltonian. This exposes limitations of the DFT + U scheme, coupled with linear response evaluation of U: in spite of a good description of ground-state properties (evaluation of total energy differences for redox potentials), only a qualitative improvement in evaluation of unoccupied states is obtained. On the other hand, it should be noted that this example demonstrates that fitting the values of electronic gaps, obtained by using DFT + U calculations to experimental data might not result in accurate description of ground-state properties.

Similar to $LiFePO_4$, we find that for the other four materials, where redox potentials have been evaluated with reasonable accuracy ($NaFePO_4$, $LiCoO_2$, $LiCoPO_4$, and $LiMnPO_4$), the DFT + U calculations lead to widening of a forbidden gap. In the same vein for the deintercalated cases of respective oxides and phosphates ($FePO_4$, CoO_2, $CoPO_4$, and $MnPO_4$), the DFT + U calculations result in a greater opening of gaps.

We have also performed a comparison of magnetic moments on transition-metal ions in the studied structures with the results of previous calculations and experimental measurements. Zhou *et al.* performed the study of intercalated and deintercalated phosphate materials and also provided the values of magnetic moments on respective transition-metal ions [56]. Overall, we find a good agreement with their work. For instance, for the three representative intercalated structures ($LiFePO_4$, $LiMnPO_4$, and $LiCoPO_4$), we find the following magnetic moments: 3.68, 4.54, and 2.67 μ_B, respectively. For comparison, Zhou *et al.* reported the values of 3.73, 4.65, and 2.78 μ_B. For respective deintercalated models, our calculations reveal the following magnetic moments: 4.21, 3.86, and 3.14 μ_B. These again are in good agreement with the respective values, reported by Zhou *et al.* (namely, 4.33, 3.95, and 3.24 μ_B).

Comparison with experimental measurements is more problematic, as the measured values of magnetic moments, reported by various groups for each specific material, may differ significantly. For instance, in case of $LiFePO_4$, magnetic moments in the range of 3.8–6.8 μ_B have been reported [57–59]. For studied materials, we find that significantly larger values of magnetic moments on transition-metal ions are determined experimentally (e.g., 5.4 and 5.1 μ_B for $LiMnPO_4$ and $LiCoPO_4$ respectively [59]). These results indicate that DFT + U calculations do not seem capable to yield magnetic moments in a good agreement with experiment. Other extensions of the theory (e.g., inclusion of magnetic exchange interactions) might be necessary for more accurate prediction of the magnetic structure of these materials [34].

Finally, we wish to analyze the underlying reasons of less accurate agreement of theoretical redox potential of $LiNiO_2$ with experiment, when DFT + U calculations are employed (Fig. 2). Our DFT + U calculations predict $LiNiO_2$ to be a metal as the Fermi level crosses PDOS of d electrons of Ni and p electrons of O atoms (Fig. 5). The absence of a gap is accounted for by the high symmetry of electronic structure for ferromagnetic ordering. We wish to point out that earlier reports also found that DOS, evaluated using DFT + U, is characterized by the absence of the gap for this material [60]. The key reason of a less accurate description of the ground-state properties for $LiNiO_2$ can be traced to the

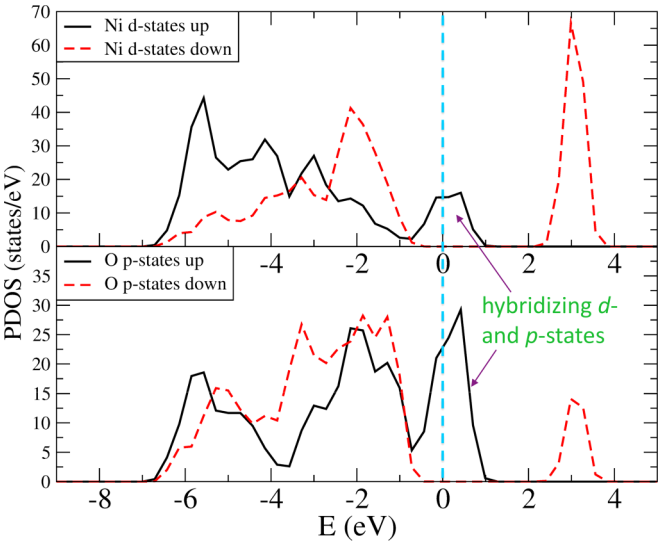

FIG. 5. PDOS of $LiNiO_2$, calculated using DFT + U method. The d states of Ni hybridize to the p states of oxygen for energies close to the Fermi level, indicated by the dashed vertical line.

pronounced hybridization of d states of Ni and p states of O as is attested by the overlap of respective peaks of PDOS close to Fermi level (Fig. 5). In this case, the orbitals, localized on Ni atoms, do not possess a close to pure d character, but also have a substantial p contribution. Therefore, the projector operator, as described in Sec. II B [Eqs. (14) and (15)], is not applied to the entire orbital, and hence cannot be used for evaluation of a complete linear response. Moreover, the Hubbard correction term [Eq. (9) in Sec. II A] is also not fully suitable for correction here and further extensions of the theory (e.g., Anderson impurity model [61] or DFT + U + V method [35]) seem to be more appropriate for adequate description of such hybridized states.

V. COMPUTATIONAL ASPECTS OF LINEAR RESPONSE METHOD

In this section, we analyze the following computational aspects of the coupled linear response/DFT + U method: (a) self-consistency in evaluation of U parameter; (b) neglect of off-diagonal elements in the response functions, used for evaluation of U; (c) linearity of density variation in response to applied potential; (d) the impact of various PAW potentials of transition metals on converged values of U and the magnitude of redox potential. Such analysis is deemed necessary for future applications of linear response/DFT + U method, as it allows to formulate the recommendations, that should be followed for correct application of the technique and adequate interpretations of the obtained results. Discussion of each listed aspect is provided in the following.

A. Self-consistency in evaluation of U parameter

U parameters are evaluated through the chain of coupled DFT + U/linear response (LR) calculations, which can be schematically illustrated as

$$\mathrm{DFT/LR} \xrightarrow{U_1} \mathrm{DFT} + U_1/\mathrm{LR} \xrightarrow{U_2} \mathrm{DFT} + U_2/\mathrm{LR} \xrightarrow{U_3} \dots . \tag{19}$$

In expression (19), we present three steps (iterations), starting from $U = 0$ (DFT). Each step consists of a solution of DFT/DFT + U system of equations with subsequent evaluation of U using the linear response approach as discussed in Sec. II B. The U parameter, determined using the LR approach, is passed on to the next step of DFT + U calculations, that can be followed by the LR calculation of a subsequent U parameter. As an example, in Fig. 6 we provide the values of U for several iterations for the case of $LiFePO_4$. The U value is found to oscillate from iteration to iteration, resulting in convergence after six to seven iterations. It should be noted that using $U = 0$ eV as a starting point is not necessary. In fact, relying on a reasonable educated guess for a starting value of U can be a better choice that allows for reaching convergence with a smaller number of iterations. The latter approach is reliable as we performed the tests, which show that a starting value of U parameter does not affect a finally converged value of U.

With regard to dependence of total energies from U parameters, we analyzed the impact of self-consistency on the magnitude of redox potentials of battery cathodes. Choosing

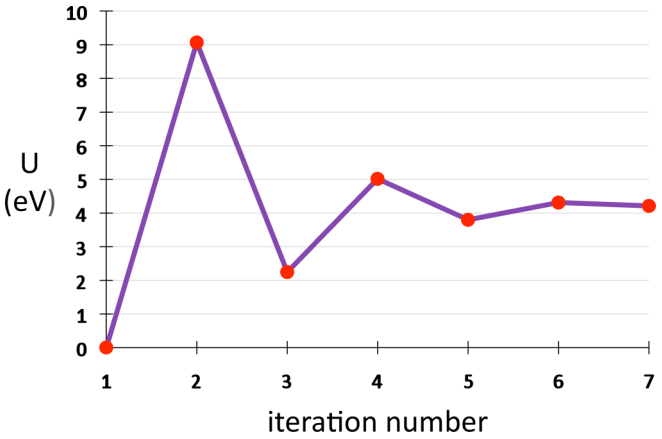

FIG. 6. The values of U parameter for $LiFePO_4$ calculated for each iteration of DFT + U/linear response calculations [Eq. (19)]. The converged value differs significantly from the U, obtained after the first iteration, which is calculated using response function of PBE density [Eq. (12)].

$LiFePO_4$ as an example, we calculated the respective redox potential, performing a single update of U (from 0 eV to the value, calculated by linear response) for both $LiFePO_4$ and $FePO_4$. The calculated value of 2.77 V is much lower than experimentally found (3.5 V [62]). However, as is shown in Fig. 2, when using self-consistently evaluated U values for $LiFePO_4$ and $FePO_4$, we find a much better agreement of redox potential with experiment.

These results show that self-consistent evaluation of U is certainly necessary for precise calculations of ground-state properties of transition-metal oxides and phosphates. This finding can be explained by a rather inaccurate description of a density and its response functions when PBE calculations are employed for analysis of these materials. Indeed, a qualitatively erroneous prediction of a metallic character of intercalated materials results in a rather inaccurate value of U, which is determined using response functions of PBE-derived densities. However, when self-consistency is applied, the U parameter is determined on the basis of DFT + U calculations, which are capable to provide more adequate response functions.

B. Neglect of off-diagonal elements in the response function, used for evaluation of U

The linear response function is in principle a matrix, defined in Eq. (13), where the density response is determined not only for the atoms on which perturbation is applied (diagonal elements), but also for other atoms of the computational cell (off-diagonal elements). Using our implementation we find that neglecting off-diagonal elements, we can still get quite reasonable values of redox potentials (Fig. 2). This is explained by rather small values of off-diagonal elements as compared to their diagonal counterparts. Using $NaFePO_4$ as an example, we find that for linear response calculations (where U is first obtained self-consistently, neglecting off-diagonal elements of response functions), the off-diagonal elements are by at least 5×10^{-3} smaller than diagonal elements. This results in a very small change of U parameter (from 4.07 to 4.10 eV), when U

is reevaluated by inversion of the complete response matrices without neglecting off-diagonal elements, indicating that the discussed approximation is justifiable.

The weak contribution of the off-diagonal elements of a response matrix, found in our calculations, is somewhat in contrast with previous works, where contribution of off-diagonal elements was found to make a greater impact on U values [22]. The key reason for greater relative values of these off-diagonal elements in previous works is the usage of DFT based densities for evaluation of the response matrices as opposed to DFT + U based density responses that where employed herein. Indeed, delocalized d-electron densities, predicted on the basis of conventional DFT calculations, are strongly perturbed on the transition-metal ions, adjacent to the ion on which linear response perturbation [Eq. (15)] is applied. On the other hand, in case of DFT + U calculations where a higher degree of localization of d electrons is imposed, the impact of perturbation [Eq. (15)] on the densities of adjacent transition-metal ions is much smaller, thus justifying complete neglect of the off-diagonal elements of response matrices when self-consistent evaluation of a U parameter is employed. Once again, using $NaFePO_4$ as an example, we find that for both self-consistent and non-self-consistent responses, the ratio of the diagonal element of the response function to the largest off-diagonal element is by 10–15 times greater when DFT + U calculations are employed as compared to the case when conventional DFT calculations are used.

C. Linearity of density variation in response to applied potential

For evaluation of density response to applied projector potential [Eq. (15)], we used a value of parameter α equal to 0.1 eV. By varying the magnitude of α, we have monitored the change of self-consistent and frozen response functions, thereby analyzing linearity of density variation as a function of applied perturbation (the off-diagonal elements of respective matrices have been neglected). For the case of $NaFePO_4$, we used five values of parameter α (0.05, 0.1, 0.2, 0.5, and 1.0 eV), which have been used as weights of applied projector operator [Eq. (15)]. For both types of response (self-consistent and frozen density) and for each chosen magnitude of α, we performed two linear response calculations: adding a projector to the DFT + U operator and subtracting a projector. This corresponds to perturbations causing up shift and down shift of d-electron levels. The response values were taken as density variation, determined by such calculations, divided by 2α.

For α equal to 0.05, 0.1, 0.2, 0.5, and 1.0 eV, the linear response calculations provide the following values of U: 4.07, 4.07, 4.11, 4.20, and 4.51 eV, respectively. Thus, we observe a slow increase of U when higher magnitude of perturbation is used. We find that for value of α below 0.1 eV, the magnitude of U changes by less than 0.01 eV. On the basis of this analysis, we can state that the value of α equal to 0.1 eV (or slightly lower, e.g., 0.05 eV) can be recommended for accurate calculations of linear response functions using Eq. (15). In passing, we wish to point out that this value is a bit smaller than those used in the published works (0.2–0.5 eV) [22]. Such difference might be attributed to different types of PAW potentials (e.g., potential radii), which results in a slightly different dependence of linear response functions from perturbation parameter α.

D. Impact of various PAW potentials of transition metals on converged values of U and the magnitude of redox potential

As mentioned in previous sections, two types of PAW potentials can be used for transition-metal atoms, present in studied structures: those with minimal number of electrons treated as valence (PAW_{min}) and potentials, which also include second outward shell (semicore) electrons as valence (PAW_{max}). Clearly, potentials with even greater number of electrons, treated as valence, can also be constructed, but these are not available for testing to date. In Table I, we provide the results of our calculations, namely, self-consistently evaluated U parameters (for intercalated and deintercalated materials) and resulting redox potentials. The calculations have been performed for both types of PAW potentials for comparison. Overall, we find that generally PAW_{max} provides redox potentials in a slightly better agreement with experiment.

A remarkable fact is a substantial difference between U parameters, which are evaluated for these two different types of PAW potentials for the same material (Table I). Indeed, such difference is within several eV. This shows a substantial impact of inclusion of semicore electrons in linear response calculations. Thus, we find that U parameters, calculated using linear response, can only be used with the same PAW potentials for subsequent DFT + U calculations. Therefore, caution needs to be exercised when U parameters are adopted from literature sources. A proper agreement between computational settings of linear response and DFT + U calculations (e.g., properties of PAW potentials) have to be ensured for obtaining adequate results.

VI. REDOX POTENTIALS: COMPARISON WITH PUBLISHED DATA

Redox potentials have been evaluated previously using DFT + U [21] as well as hybrid functional methods [16,55]. In this section, we are aiming to provide a comparison between some of these findings and our results. By analyzing the results of DFT + U and hybrid functional calculations, Chevrier *et al.* determined that DFT + U method generally yields values of redox potentials in a closer agreement with experiment as compared to HSE06 [16]. On the other hand, the HSE06 method was found to provide more accurate description of other properties (such as bond lengths and lattice constants). In a more recent work, Seo *et al.* have shown that very accurate values of redox potentials can be obtained if a fraction of exact exchange contribution in the original HSE06 is adjusted to obtain a desired property of interest [55]. In this section, we limit a comparison of our calculated redox potentials with the results determined by a linear response technique, namely, the work of Zhou *et al.* [21]. This comparison seems the most appropriate as the linear response method has been applied in our work and the work of Zhou *et al.* and no adjustable parameters have been used.

Our evaluated values of U parameters and redox potentials are presented in Table I. We start a comparison by analyzing

TABLE I. The calculated U parameters for all studied intercalated and deintercalated structures, as well as corresponding redox potentials. The results for two types of PAW potentials (PAW_{max} and PAW_{min}) are grouped in sets of four columns. For the case of PAW_{max} these are (a) scLR: results, determined by self-consistent linear response/DFT + U calculations; (b) Ave.: calculations, performed using averaged U parameters for intercalated and deintercalated structures, obtained by using scLR method; (c) Lit. ave.: calculations, performed using averaging of U parameters, reported by Zhou *et al.* [21]; (d) DFT: standard DFT calculations, where $U = 0$ for both intercalated and deintercalated structures. Then, for the case of PAW_{min}: (a) scLR: results, determined by self-consistent linear response DFT + U calculations; (b) Ref. [21]: calculations, performed using U parameters, reported by Zhou *et al.* [21]; (c) Lit. ave.: calculations, performed using averaging of U parameters, reported by Zhou *et al.* [21]; (d) DFT: standard DFT calculations, where $U = 0$ for both intercalated and deintercalated structures. The experimental redox potentials (last column) are also provided for comparison with calculated values. For materials that have not been analyzed by Zhou *et al.* ($LiTiS_2$ and $NaFePO_4$), the respective U and redox potentials are not provided.

Material properties	PAW_{max}				PAW_{min}				Expt.
	scLR	Ave.	Lit. ave.	DFT	scLR	Ref. [21]	Lit. ave.	DFT	Φ_r(V)
$U(LiTiS_2)$ (eV)	5.48	5.61		0.0	3.34			0.0	
$U(TiS_2)$ (eV)	5.73	5.61		0.0	3.54			0.0	
Φ_r (V)	1.85	1.69		1.84	2.19			1.88	2.1 [63]
$U(NaFePO_4)$ (eV)	4.07	4.96		0.0	2.19			0.0	
$U(FePO_4)$ (eV)	5.84	4.96		0.0	3.72			0.0	
Φ_r (V)	3.11	3.08		2.16	3.18			2.35	3.0 [64]
$U(LiFePO_4)$ (eV)	4.15	5.0	4.3	0.0	2.14	3.71	4.3	0.0	
$U(FePO_4)$ (eV)	5.84	5.0	4.3	0.0	3.72	4.90	4.3	0.0	
Φ_r (V)	3.61	3.03	2.99	2.68	3.72	3.76	3.47	2.87	3.5 [62]
$U(LiNiO_2)$ (eV)	5.29	5.07	6.37	0.0	4.57	6.70	6.37	0.0	
$U(NiO_2)$ (eV)	4.85	5.07	6.37	0.0	3.95	6.04	6.37	0.0	
Φ_r (V)	3.43	3.66	3.93	3.09	3.26	3.65	3.91	3.14	3.85 [65]
$U(LiMnPO_4)$ (eV)	4.39	4.89	4.51	0.0	2.19	3.92	4.51	0.0	
$U(MnPO_4)$ (eV)	5.39	4.89	4.51	0.0	3.98	5.09	4.51	0.0	
Φ_r (V)	4.29	4.01	3.93	2.95	4.22	4.31	3.99	2.99	4.1 [66]
$U(LiCoO_2)$ (eV)	4.87	5.0	5.14	0.0	3.60	4.91	5.14	0.0	
$U(CoO_2)$ (eV)	5.14	5.0	5.14	0.0	3.87	5.37	5.14	0.0	
Φ_r (V)	4.15	3.98	3.99	3.35	4.03	4.16	3.91	3.37	4.1 [67]
$U(LiCoPO_4)$ (eV)	3.52	4.29	5.70	0.0	2.81	5.05	5.70	0.0	
$U(CoPO_4)$ (eV)	5.05	4.29	5.70	0.0	4.20	6.34	5.70	0.0	
Φ_r (V)	4.87	4.33	4.48	3.76	4.78	5.00	4.71	3.83	4.8 [68]

the results of DFT calculations ($U = 0$). For $LiFePO_4$, $LiNiO_2$, $LiMnPO_4$, $LiCoO_2$, and $LiCoPO_4$, Zhou *et al.* reported redox potentials of 3.0, 3.2, 3.0, 3.8, and 3.7 V, respectively (these values are taken from the graphs provided in Ref. [21]). Except for $LiCoO_2$, we find a good agreement (within 0.1 V) with our respective values (Table I) when PAW_{min} potentials are adopted for transition metals. A small difference in redox potentials might be attributed to different sources of experimental data that have been used in our works. If PAW_{max} potentials are used, we generally observe a slightly greater disagreement for the respective materials [as the paper of Zhou *et al.* has been published more than a decade ago, we assume that potentials with minimal possible number of electrons treated as valence (e.g., PAW_{min}) have been employed]. For the case of $LiCoO_2$, a larger disagreement of DFT derived redox potentials takes place (see Table I). This greater difference might be possibly caused by different employed models of deintercalated structure (CoO_2). Relying on the findings of Amatucci *et al.* [67], we used a model of CoO_2 isostructural to CdI_2 (O1 symmetry) as opposed to a mere removal of Li atoms and relaxation of the obtained structure (O3 symmetry). This is, however, only a possible reason, as the paper of Zhou does not specify on the type of employed deintercalated structure for this case.

Now, we proceed to comparison of our findings, based on DFT + U calculations with respective results, obtained by Zhou *et al.* [21]. From the data, presented in Table I no agreement can be observed between our calculated U parameters and those reported by Zhou *et al.* [21]. This applies to intercalated and deintercalated structures for both types of PAW potentials (PAW_{min} and PAW_{max}). It should be noted that no agreement takes place between the U parameters, calculated by us based on the response functions of the PBE density (non-self-consistent calculation of U) and values, determined by Zhou *et al.* For instance, the respective U parameter, calculated by us for the case of $LiFePO_4$ is 9.1 eV (Fig. 6), which is quite different from the value of 3.71 eV reported by Zhou *et al.* (Table I). This disagreement is most likely attributed to different types of PAW potentials used in our works for linear response calculations, which includes possible differences in potential radii for transition-metal atoms, types of projectors, and the number of electrons, treated as valence. Indeed, as discussed in the previous section, employing two different PAW potentials (PAW_{min} and PAW_{max}) we obtain substantially different values of U parameters using the same VASP code (Table I).

For calculation of redox potentials, Zhou *et al.* used the total energies of intercalated and deintercalated materials

determined by DFT + U calculations with averaged U parameter for both intercalated and deintercalated structures [21]. The averaged U parameter has been obtained as a mean value of U, determined by linear response method for intercalated and deintercalated cases. This approach is different from ours where the energies of formula unit in Eq. (18) are calculated using respective values of U. In order to perform a comparison, we have evaluated redox potentials using averaged U, reported by Zhou *et al.* when PAW_{min} potentials are employed. Additionally, we have also calculated the redox potentials, using averaged U, determined from our values of U parameters for the case of PAW_{max} potentials (Table I).

Using averaged U values, provided by Zhou *et al.*, we find a close agreement of redox potentials with experimental values for $LiFePO_4$, $LiMnPO_4$, $LiNiO_2$, and $LiCoPO_4$ when PAW_{min} potentials are employed for transition-metal ions (Table I). A larger discrepancy takes place for the case of $LiCoO_2$. These findings are in line with the results of Zhou *et al.*, who also observed a less accurate theoretical redox potential for $LiCoO_2$ [21]. On the other hand, if the respective values of U, determined by Zhou *et al.* for intercalated and deintercalated materials are employed for redox potential evaluation [Eq. (18)], the agreement with experiment is lower (Table I, PAW_{min} potentials). Indeed, deviation of the theoretical redox potential from experimental values is about 0.2 V in this case. Using self-consistent linear response/DFT + U calculations and PAW_{min} potentials, we obtained a good agreement of theoretical redox potential for $LiMnPO_4$, $LiCoO_2$, and $LiCoPO_4$, whereas for $LiFePO_4$ the agreement is lower. We have already explained the reasons of very poor agreement of redox potential for the case of $LiNiO_2$ (Sec. IV).

In the case when PAW_{max} potentials are adopted and averaged U values, reported by Zhou *et al.,* are used, a lower agreement of calculated redox potentials with experiment is observed (Table I). This applies particularly to the cases of $LiFePO_4$ and $LiCoPO_4$. This indicates that adopting U parameters from published works has to be done with caution. We also find that calculations, based on averaged U parameters, evaluated using self-consistently determined U with PAW_{max} potentials, are not capable to yield accurate redox potentials in a reasonable agreement with experiment (Table I). Particularly for $LiFePO_4$ and $LiCoPO_4$, the agreement is rather poor (Table I), indicating that averaging of U parameters does not lead to a good prediction of electrochemical properties if PAW_{max} are employed.

Thus, we find that U parameters, reported in the work of Zhou *et al.* [21], can be used for obtaining reasonably accurate redox potentials if PAW_{min} potentials are utilized. However, averaging of U values for intercalated and deintercalated limits is necessary in this case. On the other hand, if self-consistent linear response/DFT + U calculations are employed, a good agreement with experimental redox potentials can be achieved if respective U parameters for intercalated and deintercalated structures are used. This indicates that U parameters, determined through self-consistent procedure, can possibly provide a more adequate electronic structure of strongly correlated materials as compared to U values, obtained by averaging between the intercalated and deintercalated limits.

VII. CONCLUSIONS

Coupled linear response/DFT + U methodology is formulated and applied to the study of ground-state properties of seven strongly correlated atomic systems, which include transition-metal elements. We find that only self-consistently determined U parameters, that are evaluated through the chain of consecutive linear response/DFT + U steps, are capable to yield redox potentials in a good agreement with experiment. By contrast, U parameters, obtained from response functions of the density, determined by conventional DFT calculations, fail to yield adequate redox potentials.

We also found that linear response functions and hence U parameters heavily depend on the type of PAW potentials for transition-metal elements, used in calculations. Therefore, adopting of U parameters, evaluated using linear response for subsequent DFT + U calculations, has to be made with caution. Additionally, we found that neglecting off-diagonal elements in response functions, used in construction of U parameters is generally justifiable, at least for the systems we analyzed herein. However, further studies of other materials, particularly those that include structural defects (e.g., vacancies or interstitials) are needed to analyze the reliability of this approach.

Our DFT + U calculations coupled with linear response method were capable to yield redox potentials with the best agreement to experiment for insulating materials with ionic bonding. These are $NaFePO_4$, $LiFePO_4$, $LiMnPO_4$, $LiCoO_2$, and $LiCoPO_4$. The computational scheme is quite successful for materials where electrons, localized on transition-metal atoms, possess nearly a pure d-electron distribution. It should be noted, however, that we have also found that for these cases DFT + U/linear response calculations provide only a qualitative improvement of description of unoccupied states. Indeed, unlike DFT calculations that erroneously predict metallic character for these materials, the DFT + U calculations lead to opening of a gap, albeit the width of this gap is still below experimental value, as is shown for the case of $LiFePO_4$.

The accuracy of evaluated redox potential is lower for the systems where d states of transition metal hybridize with p states of neighboring oxygens (e.g., $LiNiO_2$). The pd hybridization results in inaccurate response functions, leading to a U parameter that yields a value of redox potential, smaller than experimental. We believe that further extensions of the theory (DFT + U + V [35] or Anderson impurity model [61]) should be applied for such cases. Finally, we determined that even for conducting materials such as $LiTiS_2$, coupled DFT + U/linear response approach can still provide an accurate value of redox potential. Given a known metallic character of $LiTiS_2$, this material is usually treated using conventional DFT calculations [16]. However, we find that application of the DFT + U approach does not lead to erroneous prediction of insulating character for this material. Moreover, the respective redox potential is even slightly closer to experimental value, as compared to a conventional DFT result.

In summary, we have demonstrated that a self-consistently applied DFT + U/linear response method can be very useful for analysis of ground-state properties of strongly

correlated systems. The technique does not require any empirical parameters and therefore can be used for materials, characterized by a scarcity of available experimental data. Application to the study of a wider range of materials as well as evaluation of other properties of interest (e.g., oxide formation energies, etc.) can be performed in the future. These future efforts can contribute to better understanding of important characteristics of studied materials as well as to further development of the coupled DFT + U/linear response methodology.

ACKNOWLEDGMENTS

This work was performed under a management of Elements Strategy Initiative for Catalysts and Batteries (ESICB), and financial support is acknowledged.

[1] P. Hohenberg and W. Kohn, Phys. Rev. **136**, B864 (1964).
[2] W. Kohn and L. J. Sham, Phys. Rev. **140**, A1133 (1965).
[3] R. O. Jones and O. Gunnarsson, Rev. Mod. Phys. **61**, 689 (1989).
[4] M. C. Payne, M. P. Teter, D. C. Allan, T. A. Arias, and J. D. Joannopoulos, Rev. Mod. Phys. **64**, 1045 (1992).
[5] V. M. Bermudez, Surf. Sci. **579**, 11 (2005).
[6] I. R. Shein, R. Wilks, A. Moewes, E. Z. Kurmaev, D. A. Zatsepin, A. I. Kukharenko, and S. O. Cholakh, Physics of Solid State **50**, 615 (2008).
[7] C. Adamo and D. Jacquemin, Chem. Soc. Rev. **42**, 845 (2013).
[8] J. P. Perdew and A. Zunger, Phys. Rev. B **23**, 5048 (1981).
[9] J. P. Perdew and Y. Wang, Phys. Rev. B **33**, 8800 (1986).
[10] W.-K. Leung, R. J. Needs, G. Rajagopal, S. Itoh, and S. Ihara, Phys. Rev. Lett. **83**, 2351 (1999).
[11] A. J. Cohen, P. M. Sanchez, and W. Yang, Chem. Rev. **112**, 289 (2012).
[12] C. Wolverton and V. Ozolins, Phys. Rev. B **73**, 144104 (2006).
[13] V. Stevanovic, S. Lany, X. Zhang, and A. Zunger, Phys. Rev. B **85**, 115104 (2012).
[14] J. Heyd, G. E. Scuseria, and M. Ernzerhof, J. Chem. Phys. **118**, 8207 (2003).
[15] V. I. Anisimov and O. Gunnarsson, Phys. Rev. B **43**, 7570 (1991).
[16] V. L. Chevrier, S. P. Ong, R. Armiento, M. K. Y. Chan, and G. Ceder, Phys. Rev. B **82**, 075122 (2010).
[17] C. Loschen, J. Carrasco, K. M. Neyman, and F. Illas, Phys. Rev. B **75**, 035115 (2007).
[18] A. N. Andriotis, G. Mpourmpakis, S. Lisenkov, R. M. Sheetz, and M. Menon, Phys. Status Solidi B **250**, 356 (2013).
[19] I. V. Solovyev, P. H. Dederichs, and V. I. Anisimov, Phys. Rev. B **50**, 16861 (1994).
[20] W. E. Pickett, S. C. Erwin, and E. C. Ethridge, Phys. Rev. B **58**, 1201 (1998).
[21] F. Zhou, M. Cococcioni, C. A. Marianetti, D. Morgan, and G. Ceder, Phys. Rev. B **70**, 235121 (2004).
[22] M. Cococcioni and S. de Gironcoli, Phys. Rev. B **71**, 035105 (2005).
[23] N. J. Mosey and E. A. Carter, Phys. Rev. B **76**, 155123 (2007).
[24] N. J. Mosey, P. Liao, and E. M. Carter, J. Chem. Phys. **129**, 014103 (2008).
[25] L. A. Agapito, S. Curtarolo, and M. Buongiorno Nardelli, Phys. Rev. X **5**, 011006 (2015).
[26] F. Aryasetiawan, K. Karlsson, O. Jepsen, and U. Schönberger, Phys. Rev. B **74**, 125106 (2006).
[27] K. Karlsson, F. Aryasetiawan, and O. Jepsen, Phys. Rev. B **81**, 245113 (2010).
[28] R. Sakuma and F. Aryasetiawan, Phys. Rev. B **87**, 165118 (2013).
[29] K. Yu and E. Carter, J. Chem. Phys. **140**, 121105 (2014).
[30] P. Giannozzi *et al.*, http://www.quantum-espresso.org.
[31] http://cms.mpi.univie.ac.at/vasp/vasp/vasp.html.
[32] B. Himmetoglui, A. Floris, S. de Gironcolo, and M. Cococcioni, Int. J. Quantum Chem. **114**, 14 (2014).
[33] H. J. Kulik, M. Cococcioni, D. A. Scherlis, and N. Marzari, Phys. Rev. Lett. **97**, 103001 (2006).
[34] B. Himmetoglu, R. M. Wentzcovitch, and M. Cococcioni, Phys. Rev. B **84**, 115108 (2011).
[35] V. L. Campo, Jr., and M. Cococcioni, J. Phys.: Condens. Matter **22**, 055602 (2010).
[36] S. L. Dudarev, G. A. Botton, S. Y. Savrasov, C. J. Humphreys, and A. P. Sutton, Phys. Rev. B **57**, 1505 (1998).
[37] A. I. Liechtenstein, V. I. Anisimov, and J. Zaanen, Phys. Rev. B **52**, R5467 (1995).
[38] P. E. Blöchl, Phys. Rev. B **50**, 17953 (1994).
[39] O. Bengone, M. Alouani, P. E. Blöchl, and J. Hugel, Phys. Rev. B **62**, 16392 (2000).
[40] N. A. W. Holzwarth, G. E. Matthews, R. B. Dunning, A. R. Tackett, and Y. Zeng, Phys. Rev. B **55**, 2005 (1997).
[41] G. Kresse and D. Joubert, Phys. Rev. B **59**, 1758 (1999).
[42] P. E. Blöchl, C. J. Först, and J. Schimpl, Bull. Mater. Sci. **26**, 33 (2003).
[43] C. Rostgaard, arXiv:0910.1921.
[44] J. Enkovaara, C. Rostgaard, J. J. Mortensen, J. Chen *et al.*, J. Phys.: Condens. Matter **22**, 253202 (2010).
[45] S. L. Adler, Phys. Rev. **126**, 413 (1962).
[46] N. Wiser, Phys. Rev. **129**, 62 (1963).
[47] Q. Wu and T. Van Voorhis, Phys. Rev. A **72**, 024502 (2005).
[48] M. K. Aydinol, A. F. Kohan, G. Ceder, K. Cho, and J. Joannopoulos, Phys. Rev. B **56**, 1354 (1997).
[49] J. P. Perdew, K. Burke, and M. Ernzerhof, Phys. Rev. Lett. **77**, 3865 (1996).
[50] M. T. Czyżyk and G. A. Sawatzky, Phys. Rev. B **49**, 14211 (1994).
[51] P. Mohn, C. Persson, P. Blaha, K. Schwarz, P. Novák, and H. Eschrig, Phys. Rev. Lett. **87**, 196401 (2001).
[52] E. R. Ylvisaker, W. E. Pickett, and K. Koepernik, Phys. Rev. B **79**, 035103 (2009).
[53] A. G. Petukhov, I. I. Mazin, L. Chioncel, and A. I. Lichtenstein, Phys. Rev. B **67**, 153106 (2003).
[54] L. Castro, R. Dedryvere, M. El Khalifi, P.-E. Lippens, J. Breger, C. Tessier, and D. Gonbeau, J. Phys. Chem. C **7114**, 17995 (2010).
[55] D.-H. Seo, A. Urban, and G. Ceder, Phys. Rev. B **92**, 115118 (2015).
[56] F. Zhou, M. Cococcioni, K. Kang, and G. Ceder, Electrochem. Commun. **6**, 1144 (2004).

[57] A. Yamada, S. C. Chung, and K. HinoKuma, J. Electrochem. Soc. **148**, A224 (2001).
[58] G. Rousse, J. Rodriguez-Carvajal, S. Patoux, and C. Masquelier, Chem. Mater. **15**, 4082 (2003).
[59] M. C. Tucker, Ma. M. Doeff, T. J. Richardson, R. Finones, E. J. Cairns, and J. A. Reimer, J. Am. Chem. Soc. **124**, 3832 (2002).
[60] V. I. Anisimov, F. Aryasetiawan, and A. I. Lichtenstein, J. Phys.: Condens. Matter **9**, 767 (1997).
[61] P. W. Anderson, Phys. Rev. **124**, 41 (1961).
[62] A. K. Padhi, K. S. Nanjundaswamy, and J. B. Goodenough, J. Electrochem. Soc. **144**, 1188 (1997).
[63] M. S. Whittingham, Science **192**, 1126 (1976).
[64] P. Moreau, D. Guyomard, J. Gaubicher, and F. Boucher, Chem. Mater. **22**, 4126 (2010).
[65] C. Delmas, M. Menetrier, L. Croguennec, S. Levasseur, J. P. Peres, C. Pouillerie, G. Prado, L. Fournes, and F. Weill, Int. J. Inorg. Mater. **1**, 11 (1999).
[66] G. H. Li, H. Azuma, and M. Tohda, Electrochem. Solid State Lett. **5**, A135 (2002).
[67] G. G. Amatucci, J.-M. Tarascon, and L. C. Klein, J. Electrochem. Soc. **143**, 1114 (1996).
[68] K. Amine, H. Yasuda, and M. Yamachi, Electrochem. Solid State Lett. **3**, 178 (2000).